

Rate-equation approach for multi-level quantum systems

M. P. Liul^{1,*} and S. N. Shevchenko^{1,2}

¹*B. Verkin Institute for Low Temperature Physics and Engineering, Kharkov 61103, Ukraine*

²*V. N. Karazin Kharkiv National University, Kharkov 61022, Ukraine*

(Dated: March 16, 2023)

Strong driving of quantum systems opens opportunities for both controlling and characterizing their states. For theoretical studying of these systems properties we use the rate-equation formalism. The advantage of such approach is its relative simplicity. We used the formalism for description of a two-level system (TLS) with further expanding it on a case of a multi-level system. Obtained theoretical results have good agreement with experiments. The presented approach can also be considered as one more way to explore properties of quantum systems and underlying physical processes such as, for instance, Landau-Zener-Stückelberg-Majorana transitions and interference.

I. INTRODUCTION

Any problems related to quantum computers are very actual in modern physics [1, 2]. Superconducting qubits can be considered as very good candidates for being building blocks of these devices [3, 4, 5] since they have the following advantages [6]: it is possible to control superconducting qubits by microwaves; such systems show good performance during operations at nanosecond scales; superconducting qubits are scalable what opens opportunities to use them in lithography.

As a result we can conclude that any studying of superconducting qubits properties is very important for further growth and development of quantum computers. For example, such investigations could give useful insights for improvement of quantum logic gate operations [8] and enhancement of quantum algorithms performance in general [9].

The presented research is also important because it gives one more approach for studying of the Landau-Zener-Stückelberg-Majorana (LZSM) transitions and LZSM interferometry [10, 11, 12, 13]. LZSM transitions occur when a TLS is irradiated by a signal with the frequency which is much smaller than distance between energy levels [14]. Such a phenomenon is reflected in various scientific fields such as nuclear physics [15], quantum optics [16], chemical physics [17], solid-state physics [18], quantum information science [19]. Especially, it is possible to use such transitions for increasing tunneling rate [20, 21], controlling qubit gate operations [22], preparing quantum states [23, 24], multi-signal spectroscopy [25].

The repetition of LZSM transitions leads to LZSM interference [26, 27]. The LZSM interferometry can be used for a system description and control, what was underlined in Refs. [28, 29, 27]. LZSM interferometry allows to understand better the results of experiments which studied photon-assisted transport, conducted by periodic waves, in superconducting systems [30, 31] and in quantum dots [32, 33]. The result of interaction of a quantum system with environment is decoherence. Such an effect is reflected in behavior of interference picture [34, 35, 36, 37, 38]. Thus, information about decoherence processes can be deduced from the LZSM interference picture.

The rest of the paper is organized as follows. In Sec. II the rate-equation formalism for TLS is introduced with its expansion on multi-level systems. Sec. III is devoted to application of a considered approach to study stationary regime of a persistent current qubit, explored by authors of Ref. [34]. The analysis of the persistent current qubit dynamics was implemented in Sec. IV. In Sec. V we adopt the rate-equation formalism for describing a multi-level system, proposed in Ref. [7]. It is noticeable to mention that theoretical and experimental results are in very good agreement. In Sec. VI we make conclusions.

II. RATE-EQUATION APPROACH: FROM TWO-LEVEL SYSTEMS TO MULTI-LEVEL SYSTEMS

The authors of Refs. [34, 39] successfully described their experiment within the rate-equation formalism (see also Refs. [40, 41, 42]). In this section we give a short description of theoretical aspects of this method.

Let us firstly employ this method for a TLS with following extension of obtained results on multi-level systems. The Hamiltonian of a TLS, driven by external field can be written in the form:

$$\hat{H}(t) = -\frac{\Delta}{2}\hat{\sigma}_x - \frac{h(t)}{2}\hat{\sigma}_z, \quad (1)$$

where $\hat{\sigma}_z = \begin{pmatrix} 1 & 0 \\ 0 & -1 \end{pmatrix}$ and $\hat{\sigma}_x = \begin{pmatrix} 0 & 1 \\ 1 & 0 \end{pmatrix}$ are Pauli matrices, Δ is the level splitting, $h(t)$ is the external excitation which can be presented as follows:

$$h(t) = \varepsilon + A \sin 2\pi\nu t + \delta\varepsilon_{\text{noise}}(t). \quad (2)$$

Here ε is an energy detuning, ν and A are the frequency of the excitation field and its amplitude respectively, $\delta\varepsilon_{\text{noise}}(t)$ can be treated as the classical noise. In paper [34] the authors used white-noise model and for the LZSM transition rate they obtained (see also Refs. [43, 44, 45, 46])

$$W(\varepsilon, A) = \frac{\Delta^2}{2} \sum_n \frac{\Gamma_2 J_n^2(A/\nu)}{(\varepsilon - n\nu)^2 + \Gamma_2^2}. \quad (3)$$

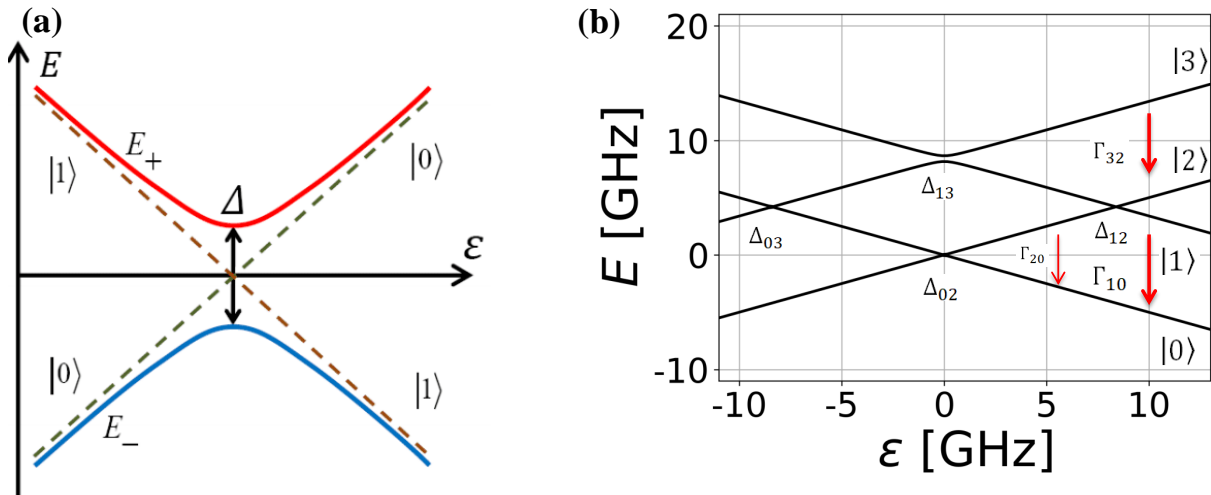


Figure 1: Energy levels as a function of the energy bias ε . Panel (a) shows graph for a TLS, (b) depicts energy levels of the four-level system studied in Ref. [7].

Here Γ_2 is the decoherence rate, J_n is the Bessel function, and the reduced Planck constant is equal to unity ($\hbar = 1$). The diagram of TLS energy levels is depicted in Fig. 1(a). Eq. (3) characterizes the transitions which happen when a system passes through a point of maximum levels convergence. In the case of a multi-level system we should assign a corresponding transition rate to each level quasicrossing point (point of maximum levels convergence). The authors of Ref. [47] proposed to extend the Eq. (3) on the transition between arbitrary states $|i\rangle$ and $|j\rangle$ of a multi-level system by the formula:

$$W_{ij}(\varepsilon_{ij}, A) = \frac{\Delta_{ij}^2}{2} \sum_n \frac{\Gamma_2 J_n^2(A/\nu)}{(\varepsilon_{ij} - n\nu)^2 + \Gamma_2^2}, \quad (4)$$

where Δ_{ij} is the energy splitting between states $|i\rangle$ and $|j\rangle$, ε_{ij} is the corresponding energy detuning. Then the rate equation for the $|i\rangle$ state can be expressed

$$\frac{dP_i}{dt} = \sum_j W_{ij}(P_j - P_i) + \sum_{i'} \Gamma_{i'i} P_{i'} - \sum_{i'} \Gamma_{ii'} P_i. \quad (5)$$

Here P_i is the probability that a system occupies $|i\rangle$ state, $\Gamma_{ii'}$ characterize the relaxation from the state $|i\rangle$ to the state $|i'\rangle$.

Thus, writing equations (5) for each level we can find occupation probabilities of the levels and then build corresponding interferograms. Usually for simplicity one considers only a stationary case, $dP_i/dt = 0$. The solution of such a system will not describe a quantum object dynamics, but it is suitable for obtaining its main properties. Also we can use the fact that the sum of all probabilities is equal to unity $\sum_i P_i = 1$.

III. QUBIT: INTERFEROGRAM

We start the studying of the rate-equation formalism from applying it to a two-level system, proposed in Ref. [34]. The considered system is a persistent-current qubit [48] described by the Hamiltonian from Eq. (1). The rate equation (5) for the system can be rewritten in the form:

$$\frac{dP_1}{dt} = W_{10}(P_0 - P_1) + \Gamma'_1 P_0 - \Gamma_1 P_1, \quad (6)$$

where Γ_1 is the relaxation rate from the state $|1\rangle$ to the state $|0\rangle$, Γ'_1 characterizes the relaxation from the state $|0\rangle$ to the state $|1\rangle$. Since we are interested in the stationary regime we can put $dP_i/dt = 0$. Supplementing Eq. (6) by the relation $P_0 + P_1 = 1$ we find:

$$P_0 = \frac{W_{10} + \Gamma_1}{2W_{10} + \Gamma_1 + \Gamma'_1}, \quad P_1 = \frac{W_{10} + \Gamma'_1}{2W_{10} + \Gamma_1 + \Gamma'_1}. \quad (7)$$

In Ref. [34] the occupation probability of an upper charge state $|1\rangle$ P_1 as a function of the flux detuning Δf (the energy detuning ε) and the source voltage V_{rms} (amplitude of the excitation field A in theory) were experimentally studied for two values of the excitation field frequency: (a) $\nu = 270$ MHz and (b) $\nu = 90$ MHz. The corresponding plot is shown in Fig. 2 of Ref. [34]. The parameters of the experiment are $\Delta = 13$ MHz, $\Gamma_1 = 50$ kHz, $\Gamma_2 = 95$ MHz, $\Gamma'_1 = \Gamma_1 \exp(-\beta\varepsilon)$, where β is a parameter which describes the relaxation from the lower level to the upper one. For our theoretical calculations we assumed $\Gamma'_1 = \Gamma_1 \times 10^{-3}$. The results of theoretical computations are presented in Fig. 2. We can conclude that theoretical and experimental plots are in a good agreement.

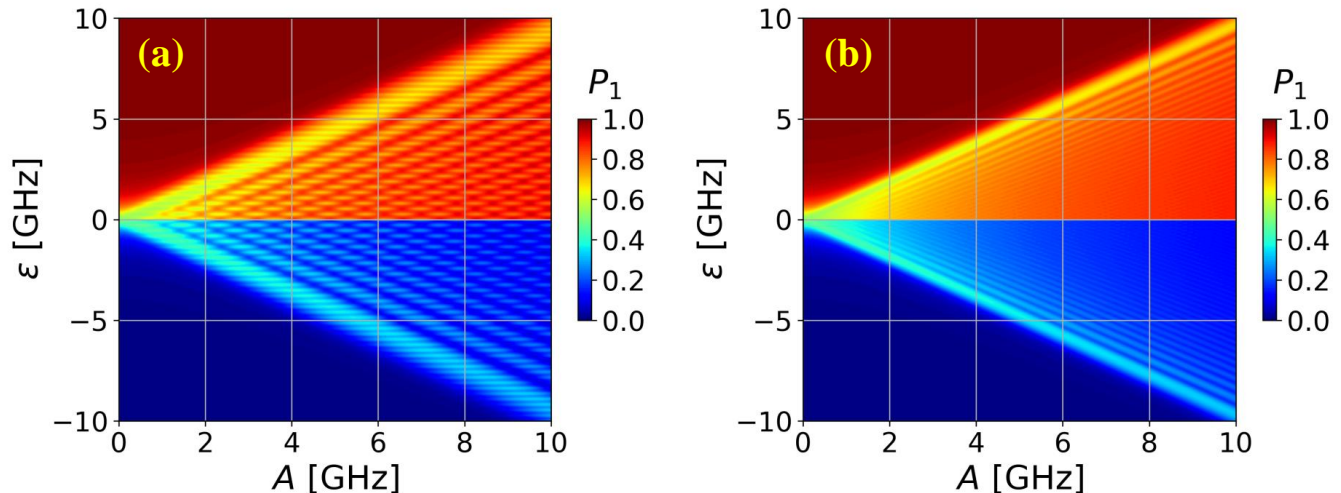


Figure 2: Population P_1 as a function of the excitation field amplitude A and the energy detuning ε . The computations were done for two different values of the excitation field frequency: (a) $\nu = 270$ MHz and (b) $\nu = 90$ MHz, in agreement with Ref. [34]. The used parameters are $\Delta = 13$ MHz, $\Gamma_1 = 50$ kHz, $\Gamma_2 = 95$ MHz, $\Gamma'_1 = \Gamma_1 \times 10^{-3}$.

IV. QUBIT: DYNAMICS

In this section a qubit dynamics is considered. For the analysis we compare two approaches: solving of the Lindblad equation (the exact solution) and the system of rate equations (the approximate one). Let us firstly describe the exact approach (see, for example, Refs. [49, 50]). The Lindblad equation with the Hamiltonian (1) can be written in the form:

$$\frac{d\rho}{dt} = -i [\hat{H}, \rho] + \sum_{\alpha} \check{L}_{\alpha}[\rho], \quad (8)$$

where $\rho = \begin{pmatrix} \rho_{00} & \rho_{01} \\ \rho_{01}^* & 1 - \rho_{00} \end{pmatrix}$ is the density matrix, such that $P_1 = 1 - \rho_{00}$, \check{L}_{α} is the Lindblad superoperator, which describes the relaxation of the system caused by interaction with the environment,

$$\check{L}_{\alpha}[\rho] = \hat{L}_{\alpha}\rho\hat{L}_{\alpha}^{\dagger} - \frac{1}{2} \left\{ \hat{L}_{\alpha}^{\dagger}\hat{L}_{\alpha}, \rho \right\}, \quad (9)$$

where $\{a, b\} = ab + ba$ is the anticommutator. For a qubit there are two possible channels of relaxation: dephasing (described by \hat{L}_{ϕ}) and energy relaxation (described by L_{relax}). The corresponding operators have the following form:

$$\hat{L}_{\text{relax}} = \sqrt{\Gamma_1}\hat{\sigma}^+, \quad \hat{L}_{\phi} = \sqrt{\frac{\Gamma_{\phi}}{2}}\hat{\sigma}_z, \quad (10)$$

where $\hat{\sigma}^+ = \begin{pmatrix} 0 & 1 \\ 0 & 0 \end{pmatrix}$, Γ_1 is the qubit relaxation, Γ_{ϕ} is the pure dephasing rate, $\Gamma_2 = \Gamma_1/2 + \Gamma_{\phi}$ is the decoherence rate.

On the one hand, by solving Eq. (8) one obtains P_1 as a function of time t , driving frequency ν and amplitude

A , energy detuning ε , the level splitting Δ . The occupation probability is the function of all these parameters, $P_1 = P_1(t, \nu, A, \varepsilon, \Delta)$. Obtained dependence allows us to build, for instance, $P_1 = P_1(\varepsilon, t)$. On the other hand, we can get the same relation by solving Eq. (5). Figs. 3 (a, b) show the results of the theoretical calculations of P_1 as a function of time t and energy detuning ε for $A = 8$ GHz and $\nu = 270$ MHz, other parameters are the same with Fig. 2. Panel (a) was calculated by the Lindblad equation approach, while (b) is the result of solving the rate equations. One can conclude that considered approaches are in a good qualitative correspondence. We also built the pictures for the $\nu = 90$ MHz but since it did not give any additional insights, it was decided not to include this case to the article. In Fig. 3 (c), we can see the line cut along Figs. 3 (a, b) at $\varepsilon = 5$ GHz (blue line) and $\varepsilon = 7.5$ GHz (black line). Solid lines correspond to the exact solution, dashed lines are solutions of the rate equations. We can see that both approaches are in a good agreement. The difference between them can be seen if to zoom pictures (for example, consider the first microseconds of the process). Fig. 3 (d) shows the dynamics of the considered process during the first 400 nanoseconds. The lines are marked in the same way as in Fig. 3 (c). From the comparison we can deduce that the rate-equation formalism averages the oscillations, so the corresponding curve is a monotonous curve, while the Lindblad equation approach reflects more sophisticated system behavior.

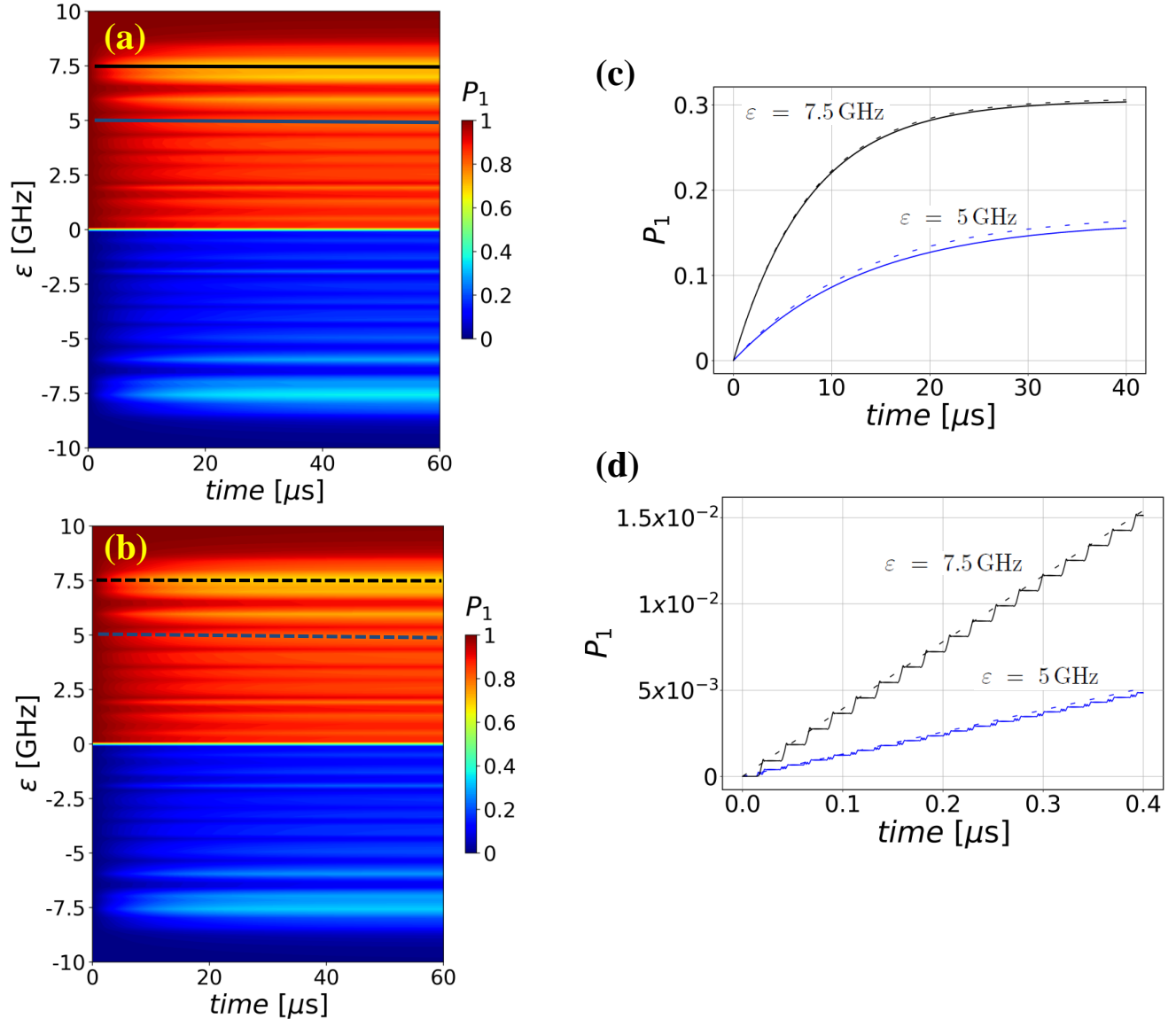


Figure 3: Population P_1 as a function of time t . Panels (a, b) show P_1 as a function of time t and energy detuning ε for $A = 8$ GHz and $\nu = 270$ MHz. Panel (a) was calculated by the Lindblad equation approach, (b) is the result of solving the rate equations. Panel (c) is the line cut along (a, b) at $\varepsilon = 5$ GHz (blue line, lower set of curves) and $\varepsilon = 7.5$ GHz (black line, upper set of curves). Solid lines correspond to the exact solution, dashed are solutions of the rate equations. Panel (d) shows the dynamics of the considered process during the first 400 nanoseconds, the lines are marked in the same way as in (c). Other parameters are the same with Fig. 2.

V. MULTI-LEVEL SYSTEMS: DYNAMICS AND INTERFEROGRAMS; THE CASE OF A SOLID-STATE ARTIFICIAL ATOM

In this section we theoretically study the solid-state artificial atom in the layout of Ref. [7]. An artificial atom is a structure where electrons are trapped and can only have discrete energy states, like in real atoms. The unperturbed part of the considered system Hamiltonian

has a form [51]:

$$H = \sum_n E_n |n\rangle\langle n| - \frac{1}{2} \sum_{m \neq n} \Delta_{mn} |m\rangle\langle n|, \quad (11)$$

for case of our system unperturbed part of the Hamiltonian can be written as

$$H = -\frac{1}{2} \begin{pmatrix} -\varepsilon - B & 0 & \Delta_{02} & \Delta_{03} \\ 0 & \varepsilon & \Delta_{12} & \Delta_{13} \\ \Delta_{02} & \Delta_{12} & -\varepsilon & 0 \\ \Delta_{03} & \Delta_{13} & 0 & \varepsilon - B \end{pmatrix}. \quad (12)$$

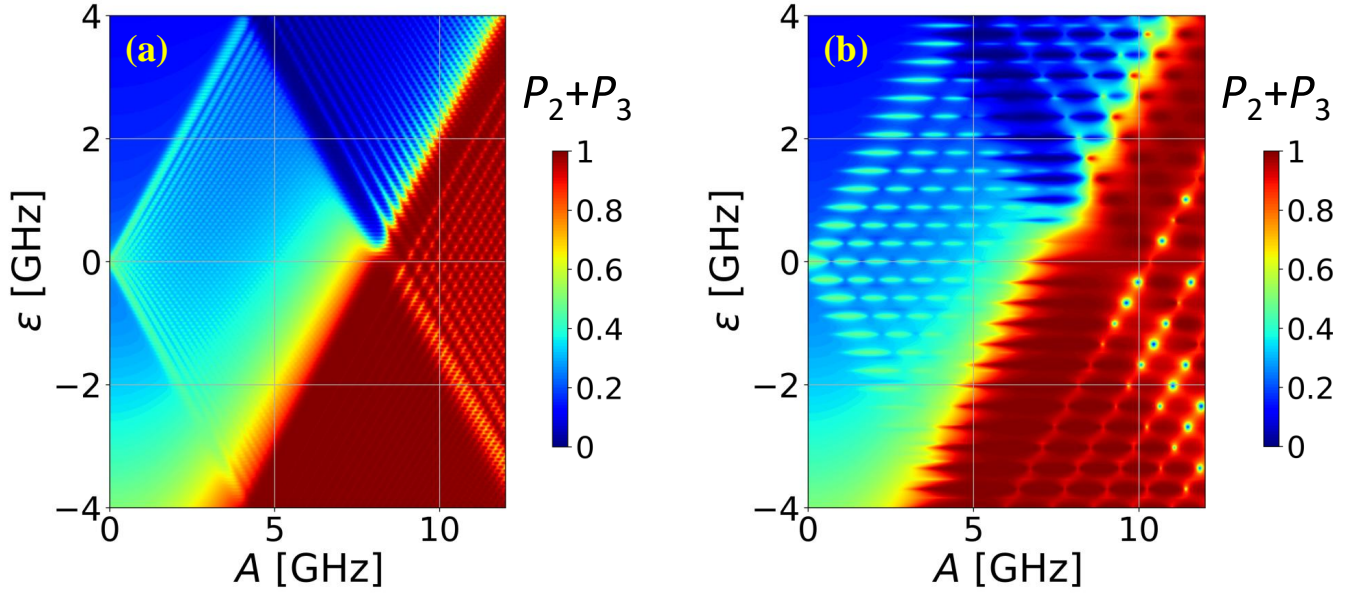


Figure 4: Artificial atom population $P_L = P_2 + P_3$ as a function of the excitation field amplitude A and the energy detuning ε . For panel (a) the driving frequency $\nu = 0.16$ GHz, for (b) $\nu = 0.85$ GHz. The corresponding relaxation rates of the system are $\Gamma_{10} = 0.6$ GHz, $\Gamma_{32} = 0.6$ GHz, $\Gamma_{20} = 0.05$ MHz. The inverse relaxation rates (from a lower state $|m\rangle$ to an upper one $|n\rangle$) are Boltzmann suppressed and for simplicity we took $\Gamma_{mn} = \Gamma_{nm}/100$. The energy splittings are equal $\Delta_{02} = 0.09$ GHz, $\Delta_{12} = 0.013$ GHz, $\Delta_{13} = 0.5$ GHz, $\Delta_{03} = 0.5$ GHz and their positions are at $\varepsilon = 0, 8.4, 0$ and -8.4 GHz respectively. The decoherence rate $\Gamma_2 = 0.05$ GHz. The system energy slopes [7] equal $|m_0|, |m_2| = 1.44, |m_1|, |m_3| = 1.09$.

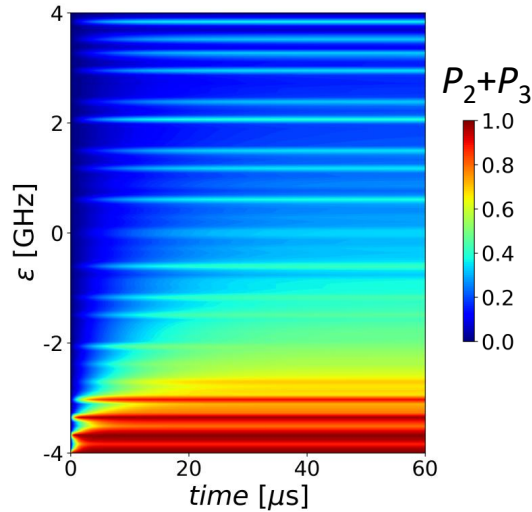


Figure 5: Artificial atom population $P_L = P_2 + P_3$ as a function of the energy detuning ε and time t . The calculations were done for $A = 4$ GHz and $\nu = 0.85$ GHz. Other parameters are the same with Fig. 4.

The value $B = 2 \times 8.4$ GHz describes the position of quasicrossings Δ_{12} and Δ_{03} (see also further in the text). The corresponding energy diagram can be seen in Fig. 1(b). The obtained energy diagram is in a good agreement with ones in Refs. [7, 47]. In the region of our interest the system contains 4 energy levels, placed in double-well potential, detailed energy configuration can be found in Ref. [45]. In the considered case states $|0\rangle$ and

$|1\rangle$ are in the right well, states $|2\rangle$ and $|3\rangle$ are in the left one. Moreover, accordingly to Ref. [7], the relaxation inside a well is faster in this solid-state artificial atom than the relaxation between wells, so one can neglect relaxations from state $|1\rangle$ to state $|2\rangle$ and vice-versa. In the experiment the population in the left well $P_L = P_2 + P_3$ was measured. Applying Eq. (5) to the analyzed system one obtains the system of rate equations:

$$\begin{cases} \dot{P}_0 = -P_0(W_{02} + W_{03} + \Gamma_{20}) + P_2(W_{20} + \Gamma_{20}) + P_1\Gamma_{10} + P_3W_{03} \\ \dot{P}_1 = -P_1(W_{12} + W_{13} + \Gamma_{10}) + P_2W_{12} + P_3W_{13} \\ \dot{P}_2 = P_0(W_{02} + \Gamma_{02}) - P_2(W_{02} + W_{12} + \Gamma_{20}) + P_3\Gamma_{23} + P_1W_{12} \\ P_0 + P_1 + P_2 + P_3 = 1. \end{cases} \quad (13)$$

The corresponding relaxation rates of the system are $\Gamma_{10} = 0.6$ GHz, $\Gamma_{32} = 0.6$ GHz, $\Gamma_{20} = 0.05$ MHz. The inverse relaxation rates (from a lower state $|m\rangle$ to an upper one $|n\rangle$) are Boltzmann suppressed and for simplicity we took $\Gamma_{mn} = \Gamma_{nm}/100$. The energy splittings are equal to $\Delta_{02} = 0.09$ GHz, $\Delta_{12} = 0.013$ GHz, $\Delta_{13} = 0.5$ GHz, $\Delta_{03} = 0.5$ GHz and their positions are at $\varepsilon = 0, 8.4, 0$ and -8.4 GHz respectively. The decoherence rate $\Gamma_2 = 0.05$ GHz.

To make the correspondence between the theory and the experiment better, the authors of Ref. [47] proposed to take into account the diabatic energy-level slope $m_i = dE_i(\varepsilon)/d\varepsilon$ of a level i with energy E_i . The Eq. (2) can be rewritten in the form:

$$h_{ij}(t) = (|m_i| + |m_j|)(\varepsilon + A \sin 2\pi\nu t) + \delta\varepsilon_{\text{noise}}(t). \quad (14)$$

The system energy slopes [7] equal $|m_0|, |m_2| = 1.44$, $|m_1|, |m_3| = 1.09$.

The results of the theoretical calculations are presented in Fig. 4. Panel (a) corresponds to the case of $\nu = 0.16$ GHz, (b) was built for driving frequency $\nu = 0.85$ GHz. The full picture consists of triangles which can be very roughly interpreted as interactions within TLS. For example, the system behaves like a qubit on the interval $A < 4$ GHz. For the case (a) the picture on the interval $A > 8.4$ GHz is also TLS-like, while for

the case (b) the system behavior is more sophisticated. We can also conclude that for the higher frequency resonances become more distinguishable as it was observed for a qubit.

To complete the research let us study the system dynamics. Fig. 5 shows a dependence of population $P_2 + P_3$ on time and energy detuning ε for $A = 4$ GHz and $\nu = 0.85$ GHz. All parameters are the same with Fig. 4.

VI. CONCLUSIONS

Description of an N -level quantum system, if solving a Master equation, requires solving $N^2 - 1$ equations for the density-matrix components. We consider an alternative approach consisting in solving the rate equations, the number of which is $N - 1$. We started from a TLS for which we have only one equation instead of three Bloch equations. Then we considered generalization for a multi-level system and described a multi-level flux-qubit-based device. The rate-equation approach involves relaxation and decoherence and is demonstrated to be convenient for obtaining the stationary states. Particularly, we have applied this method for the LZSM interferometry, which is an important tool for quantum characterization and control.

Acknowledgments

The authors acknowledge fruitful discussions with A. Ryzhov. This work was supported by Army Research Office (ARO) (Grant No. W911NF2010261).

* e-mail: liul@ilt.kharkov.ua

¹ M. A. Nielsen and I. L. Chuang, *Quantum Computation and Quantum Information: 10th Anniversary Edition* (Cambridge University Press, 2010).

² H. Haffner, C. Roos, and R. Blatt, "Quantum computing with trapped ions," *Phys. Rep.* **469**, 155–203 (2008).

³ M. H. Devoret and R. J. Schoelkopf, "Superconducting circuits for quantum information: An outlook," *Science* **339**, 1169–1174 (2013).

⁴ J. M. Gambetta, J. M. Chow, and M. Steffen, "Building logical qubits in a superconducting quantum computing system," *npj Quantum Information* **3**, 2 (2017).

⁵ G. Wendin, "Quantum information processing with superconducting circuits: a review," *Rep. Progr. Phys.* **80**, 106001 (2017).

⁶ W. D. Oliver and P. B. Welander, "Materials in superconducting quantum bits," *MRS Bulletin* **38**, 816 (2013).

⁷ D. Berns, M. Rudner, S. Valenzuela, K. Berggren, W. Oliver, L. Levitov, and T. Orlando, "Amplitude spectroscopy of a solid-state artificial atom," *Nature* **455**, 51–57 (2008).

⁸ D. L. Campbell, Y.-P. Shim, B. Kannan, R. Winik, D. K.

Kim, A. Melville, B. M. Niedzielski, J. L. Yoder, C. Tahan, S. Gustavsson, and W. D. Oliver, "Universal nonadiabatic control of small-gap superconducting qubits," *Phys. Rev. X* **10**, 041051 (2020).

⁹ E. Lucero, R. Barends, Y. Chen, J. Kelly, M. Mariantoni, A. Megrant, P. O'Malley, D. Sank, A. Vainsencher, J. Wenner, T. White, Y. Yin, A. Cleland, and J. Martinis, "Computing prime factors with a Josephson phase qubit quantum processor," *Nature Phys.* **8**, 719 (2012).

¹⁰ W. D. Oliver, Y. Yu, J. C. Lee, K. K. Berggren, L. S. Levitov, and T. P. Orlando, "Mach-Zehnder interferometry in a strongly driven superconducting qubit," *Science* **310**, 1653–1657 (2005).

¹¹ S. N. Shevchenko, S. Ashhab, and F. Nori, "Landau-Zener-Stückelberg interferometry," *Phys. Rep.* **492**, 1–30 (2010).

¹² M. Sillanpää, T. Lehtinen, A. Paila, Y. Makhlin, and P. Hakonen, "Continuous-time monitoring of Landau-Zener interference in a Cooper-pair box," *Phys. Rev. Lett.* **96**, 187002 (2006).

¹³ P. O. Kofman, O. V. Ivakhnenko, S. N. Shevchenko, and F. Nori, "Majorana's approach to nonadiabatic transitions

- validates the adiabatic-impulse approximation,” (2022).
- 14 A. Izmalkov, M. Grajcar, E. Il’ichev, N. Oukhanski, T. Wagner, H.-G. Meyer, W. Krech, M. H. S. Amin, A. M. van den Brink, and A. M. Zagoskin, “Observation of macroscopic Landau-Zener transitions in a superconducting device,” *Europhys. Lett.* **65**, 844–849 (2004).
 - 15 A. Thiel, “The Landau-Zener effect in nuclear molecules,” *J. Phys. G: Nucl. Part. Phys.* **16**, 867–910 (1990).
 - 16 D. Bouwmeester, N. H. Dekker, F. E. v. Dorsselaer, C. A. Schrama, P. M. Visser, and J. P. Woerdman, “Observation of Landau-Zener dynamics in classical optical systems,” *Phys. Rev. A* **51**, 646–654 (1995).
 - 17 L. Zhu, A. Widom, and P. M. Champion, “A multidimensional Landau-Zener description of chemical reaction dynamics and vibrational coherence,” *J. Chem. Phys.* **107**, 2859–2871 (1997).
 - 18 W. Wernsdorfer, R. Sessoli, A. Caneschi, D. Gatteschi, and A. Cornia, “Nonadiabatic Landau-Zener tunneling in Fe₈ molecular nanomagnets,” *Europhys. Lett. (EPL)* **50**, 552–558 (2000).
 - 19 G. Fuchs, G. Burkard, P. Klimov, and D. Awschalom, “A quantum memory intrinsic to single nitrogen-vacancy centres in diamond,” *Nature Phys.* **7**, 789–793 (2011).
 - 20 J. Ankerhold and H. Grabert, “Enhancement of macroscopic quantum tunneling by Landau-Zener transitions,” *Phys. Rev. Lett.* **91**, 016803 (2003).
 - 21 G. Ithier, E. Collin, P. Joyez, D. Vion, D. Esteve, J. Ankerhold, and H. Grabert, “Zener enhancement of quantum tunneling in a two-level superconducting circuit,” *Phys. Rev. Lett.* **94**, 057004 (2005).
 - 22 K. Saito and Y. Kayanuma, “Nonadiabatic electron manipulation in quantum dot arrays,” *Phys. Rev. B* **70**, 201304 (2004).
 - 23 K. Saito, M. Wubs, S. Kohler, P. Hänggi, and Y. Kayanuma, “Quantum state preparation in circuit QED via Landau-Zener tunneling,” *Europhys. Lett. (EPL)* **76**, 22–28 (2006).
 - 24 H. Ribeiro and G. Burkard, “Nuclear state preparation via Landau-Zener-Stückelberg transitions in double quantum dots,” *Phys. Rev. Lett.* **102**, 216802 (2009).
 - 25 M. A. Nakonechnyi, D. S. Karpov, A. N. Omelyanchouk, and S. N. Shevchenko, “Multi-signal spectroscopy of qubit-resonator systems,” *Low Temp. Phys.* **37**, 383 (2021).
 - 26 S. N. Shevchenko, *Mesoscopic Physics meets Quantum Engineering* (World Scientific, Singapore, 2019).
 - 27 O. V. Ivakhnenko, S. N. Shevchenko, and F. Nori, “Nonadiabatic Landau-Zener-Stückelberg-Majorana transitions, dynamics and interference,” (2022).
 - 28 L. Y. Gorelik, N. I. Lundin, V. S. Shumeiko, R. I. Shekhter, and M. Jonson, “Superconducting single-mode contact as a microwave-activated quantum interferometer,” *Phys. Rev. Lett.* **81**, 2538–2541 (1998).
 - 29 T. Wu, Y. Zhou, Y. Xu, S. Liu, and J. Li, “Landau-Zener-Stückelberg interference in nonlinear regime,” *Chin. Phys. Lett.* **36**, 124204 (2019).
 - 30 P. K. Tien and J. P. Gordon, “Multiphoton process observed in the interaction of microwave fields with the tunneling between superconductor films,” *Phys. Rev.* **129**, 647–651 (1963).
 - 31 Y. Nakamura and J. S. Tsai, “A coherent two-level system in a superconducting single-electron transistor observed through photon-assisted cooper-pair tunneling,” *J. Supercond.* **12**, 799–806 (1999).
 - 32 L. P. Kouwenhoven, S. Jauhar, J. Orenstein, P. L. McEuen, Y. Nagamune, J. Motohisa, and H. Sakaki, “Observation of photon-assisted tunneling through a quantum dot,” *Phys. Rev. Lett.* **73**, 3443–3446 (1994).
 - 33 W. J. M. Naber, T. Fujisawa, H. W. Liu, and W. G. van der Wiel, “Surface-acoustic-wave-induced transport in a double quantum dot,” *Phys. Rev. Lett.* **96**, 136807 (2006).
 - 34 D. M. Berns, W. D. Oliver, S. O. Valenzuela, A. V. Shytov, K. K. Berggren, L. S. Levitov, and T. P. Orlando, “Coherent quasiclassical dynamics of a persistent current qubit,” *Phys. Rev. Lett.* **97**, 150502 (2006).
 - 35 M. S. Rudner, A. V. Shytov, L. S. Levitov, D. M. Berns, W. D. Oliver, S. O. Valenzuela, and T. P. Orlando, “Quantum phase tomography of a strongly driven qubit,” *Phys. Rev. Lett.* **101**, 190502 (2008).
 - 36 L. Du, M. Wang, and Y. Yu, “Landau-Zener-Stückelberg interferometry in the presence of quantum noise,” *Phys. Rev. B* **82**, 045128 (2010).
 - 37 R. K. Malla and M. E. Raikh, “High Landau levels of two-dimensional electrons near the topological transition caused by interplay of spin-orbit and Zeeman energy shifts,” *Phys. Rev. B* **99**, 205426 (2019).
 - 38 R. K. Malla and M. Raikh, “Landau-Zener transition between two levels coupled to continuum,” *Phys. Lett. A* **445**, 128249 (2022).
 - 39 W. D. Oliver and S. O. Valenzuela, “Large-amplitude driving of a superconducting artificial atom,” *Quantum Inf. Process.* **8**, 261–281 (2009).
 - 40 A. Ferrón, D. Domínguez, and M. J. Sánchez, “Large-amplitude harmonic driving of highly coherent flux qubits,” *Phys. Rev. B* **82**, 134522 (2010).
 - 41 A. Ferrón, D. Domínguez, and M. J. Sánchez, “Tailoring population inversion in Landau-Zener-Stückelberg interferometry of flux qubits,” *Phys. Rev. Lett.* **109**, 237005 (2012).
 - 42 A. Ferrón, D. Domínguez, and M. J. Sánchez, “Dynamic transition in Landau-Zener-Stückelberg interferometry of dissipative systems: The case of the flux qubit,” *Phys. Rev. B* **93**, 064521 (2016).
 - 43 J.-D. Chen, X.-D. Wen, G.-Z. Sun, and Y. Yu, “Landau-Zener-Stückelberg interference in a multi-anticrossing system,” *Chin. Phys. B* **20**, 088501 (2011).
 - 44 Y. Wang, S. Cong, X. Wen, C. Pan, G. Sun, J. Chen, L. Kang, W. Xu, Y. Yu, and P. Wu, “Quantum interference induced by multiple Landau-Zener transitions in a strongly driven rf-squid qubit,” *Phys. Rev. B* **81**, 144505 (2010).
 - 45 X. Wen, Y. Wang, S. Cong, G. Sun, J. Chen, L. Kang, W. Xu, Y. Yu, P. Wu, and S. Han, “Landau-Zener-Stückelberg interferometry in multilevel superconducting flux qubit,” *arXiv* (2010).
 - 46 R. M. Otxoa, A. Chatterjee, S. N. Shevchenko, S. Barraud, F. Nori, and M. F. Gonzalez-Zalba, “Quantum interference capacitor based on double-passage Landau-Zener-Stückelberg-Majorana interferometry,” *Phys. Rev. B* **100**, 205425 (2019).
 - 47 X. Wen and Y. Yu, “Landau-Zener interference in multilevel superconducting flux qubits driven by large-amplitude fields,” *Phys. Rev. B* **79** (2009).
 - 48 T. P. Orlando, J. E. Mooij, L. Tian, C. H. van der Wal, L. S. Levitov, S. Lloyd, and J. J. Mazo, “Superconducting persistent-current qubit,” *Phys. Rev. B* **60**, 15398–15413 (1999).
 - 49 G. Lindblad, “On the generators of quantum dynamical semigroups,” *Commun. Math. Phys.* **48**, 119 – 130 (1976).
 - 50 D. Manzano, “A short introduction to the Lindblad master equation,” *AIP Adv.* **10**, 025106 (2020).

- ⁵¹ A. M. Whiticar, A. Y. Smirnov, T. Lanting, J. Whittaker, F. Altomare, T. Medina, R. Deshpande, S. Ejtemaee, E. Hoskinson, M. Babcock, and M. H. Amin, “Probing flux and charge noise with macroscopic resonant tunneling,” [arXiv \(2022\)](#).